Arias-Martorell, Julia; Urciuoli, Alessandro; Almécija, Sergio; [et al.]. «The radial head of the Middle Miocene ape Nacholapithecus kerioi : Morphometric affinities, locomotor inferences, and implications for the evolution of the hominoid humeroradial joint». Journal of Human Evolution, Vol. 178 (May 2023), art. 103345. DOI 10.1016/j.jhevol.2023.103345

Short Communication

The radial head of the Middle Miocene ape *Nacholapithecus kerioi*: Morphometric affinities, locomotor inferences, and implications for the evolution of the hominoid humeroradial joint

Julia Arias-Martorell[a,b,*], Alessandro Urciuoli[c,d,a], Sergio Almécija[e,f,a], David M. Alba[a], Masato Nakatsukasa[g]

[a] *Insitut Català de Paleontologia Miquel Crusafont, Universitat Auntònoma de Barcelona, Edifici ICTA-ICP, c/ Columnes s/n, Campus de la UAB, 08193 Cerdanyola del Vallès, Barcelona, Spain*

[b] *School of Anthropology and Conservation, Marlowe Building, University of Kent, Canterbury, CT2 7NR, UK*

[c] *Universitat Autònoma de Barcelona, Campus de la UAB, 08193 Cerdanyola del Vallès, Barcelona, Spain*

[d] *Division of Palaeoanthropology, Senckenberg Research Institute and Natural History Museum Frankfurt, Frankfurt am Main, Germany*

[e] *Division of Anthropology, American Museum of Natural History, Central Park West at 79th Street, New York, NY 10024, USA*

[f] *New York Consortium in Evolutionary Primatology, New York, NY 10024, USA*

[g] *Laboratory of Physical Anthropology, Graduate School of Science, Kyoto University, 606-8502 Kyoto, Japan*

*Corresponding author.

E-mail address: julia.arias@icp.cat (J. Arias-Martorell).

Acknowledgments

We would like to thank NACOSTI for permission to carry out this research in Kenya; we also thank the Director, Head of Earth Sciences and Palaeontology Section Staff at the National Museums of Kenya for their support and collaboration in this project. We would also like to thank the Associate Editor and three reviewers for their help improving earlier versions of this manuscript. This work is part of R+D+I projects PID2020-116908GB-I00 and PID2020-117289GBI00, funded by the Agencia Estatal de Investigación of the Spanish Ministry of Science and Innovation (MCIN/AEI/10.13039/501100011033/). Research has also been supported by the Generalitat de Catalunya/CERCA Programme, the Agència de Gestió d'Ajust Universitaris i de Recerca of the Generalitat de Catalunya (2022 SGR 01188 and 2022 SGR 00620, and Beatriu de Pinós Programme—H2020 MSCA-Cofund Grant No 801370 to J.A.M), a Margarita Salas postdoctoral fellowship funded by the European Union-NextGenerationEU to A.U, and the grants JPJSBP120216301 and KAKENHI 22H02708 to M.N.

Short Communication

The radial head of the Middle Miocene ape *Nacholapithecus kerioi*: Morphometric affinities, locomotor inferences, and implications for the evolution of the hominoid humeroradial joint

Keywords: Miocene apes; Forelimb; Elbow joint; Pronosupination; Locomotion; 3D geometric morphometrics

1. Introduction

The systematic position of the Middle Miocene large-bodied ape *Nacholapithecus kerioi* (see review in Nakatsukasa and Kunimatsu, 2009) is somewhat uncertain (e.g., Almécija et al., 2021), being considered a stem hominid by some researchers (Alba, 2012; Kunimatsu et al., 2019) but being favored as a stem hominoid by recent cladistic analyses (Pugh, 2022). The remains of this species, dated to the Middle Miocene (16 –15 Ma; Sawada et al., 1998, 2006; Nakatsukasa and Kunimatsu, 2009), were originally discovered in the Aka Aiteputh Formation of the Nachola region (northern Kenya) and assigned to *Kenyapithecus* (Ishida et al., 1984; Rose et al., 1996; Nakatsukasa et al., 1998). However, the discovery of the articulated partial skeleton KNM-BG 35250, of which numerous postcranial elements and the cranium were recovered (Nakatsukasa et al., 1998; Ishida et al., 2004), prompted the description of a new genus and species for the large-bodied hominoid from Nachola (Ishida et al., 1999).

Many postcranial elements of *N. kerioi* have been described in detail from the holotype KNM-BG 25350 skeleton (Nakatsukasa et al., 1998, 2003a, 2007b, 2012; Ishida et al., 2004; Senut et al., 2004; Kikuchi et al., 2012, 2015, 2016; Ogihara et al., 2016; Takano et al., 2018), as well as from numerous (mostly isolated) finds (Rose et al., 1996; Nakatsukasa et al., 2003b, 2007a; Pina et al., 2021; Takano et al., 2020). From these studies, it has been inferred that *N. kerioi* possessed a pronograde body plan (narrow thorax, long and flexible vertebral column, and limbs used mostly in the parasagittal plane; Nakatsukasa and Kunimatsu, 2009), like other Early and Middle Miocene apes such as *Ekembo* and *Equatorius* (see review in Ward, 2015). However, *Nacholapithecus* exhibits derived postcranial features compared with those of earlier (e.g., *Ekembo*) and contemporaneous (e.g., *Equatorius*) stem hominoids, especially in the elbow joint, which exhibits a deep zona conoidea and a large, globular, and medially tilted capitulum in the distal humerus (Nakatsukasa and Kunimatsu, 2009; Takano et al. 2020). These derived features indicate that *Nacholapithecus* displays the earliest known evidence of increased forelimb-dominated behaviors with enhanced vertical climbing capabilities among fossil apes (Nakatuskasa and Kunimatsu, 2009; Takano et al., 2018, 2020).

The distal humeral and proximal ulnar morphology of *Nacholapithecus* have been interpreted from a locomotor viewpoint (Takano et al., 2018, 2020) but its proximal radial morphology remains to be analyzed from this perspective. The distinctively derived proximal radial morphology of extant hominoids is functionally related to wide ranges of pronosupination coupled with universal stability at the humeroradial joint (Sarmiento, 1988; Rose, 1988, 1993; Sarmiento et al., 2002: Fig. 4) and has been used to make locomotor inferences in fossil catarrhines (Arias-Martorell et al., 2021). Therefore, here we provide a quantitative morphological analysis of the radial head of *N. kerioi* with the objective of refining previous locomotor inferences for this species. Our analysis is based on the isolated proximal radius fragment KNM-BG 40021 from the fossiliferous site BG-K (see Takano et al., 2020 for a full description of the specimen). We compare it with stem catarrhines and other Miocene hominoids by means of three-dimensional geometric morphometrics (3DGM) to establish its closest morphometric affinities.

2. Materials and methods

2.1. Studied and comparative sample

The right proximal radial fragment of *N. kerioi* KNM-BG 40021 (Fig. 1; Takano et al., 2020) is housed at the National Museums of Kenya (KNM, Nairobi, Kenya). KNM-BG 40021 is a 63 mm-long fragment preserving the radial head, radial tuberosity, and a small section of the shaft below the radial tuberosity. The specimen has compression damage affecting mainly the shaft and radial tuberosity, which are both flattened anteroposteriorly. The posterior aspect of the radial head is also flattened, affecting the depth of the fovea, which shows an artifactually increased depth. However, the anterior and medial/lateral aspects of the radial head are well-preserved and preserve their original morphology, including the outline of the fovea (Takano et al., 2020). Our analyses focused on this undistorted and well-preserved aspect of the radial head, the shape of which we characterized using 3DGM to capture more subtle aspects of variation such as the curvature and outline of the radial head, which are very important aspects of radial head variation and function.

The comparative fossil sample includes 3D virtual models of the radii of the dendropithecids *Simiolus enjisessi* and *Dendropithecus macinessi*, the pliopithecoid *Epipliopithecus vindobonensis*, and the stem hominoids *Ekembo heseloni* and *Equatorius africanus* (see Supplementary Online Material [SOM] Table S1 for further details). The extant comparative sample is the same as in Arias-Martorell et al. (2021), including 116 radii from 26 anthropoid species including all extant hominoid genera (SOM Table S2). Three-dimensional landmarks were collected from 3D models of the radii listed in SOM Tables S1 and S2. Details about the scanning procedures of both the fossil and extant comparative sample are presented in SOM S1 and SOM Table S2. All 3D models from right radii (including fossils) were mirrored to the left side during the process of mesh reconstruction as most extant anthropoid radii in our sample are from the left side. Landmarks were placed using IDAV Landmark Editor v. 3.6 (Wiley et al., 2005) and all statistical analysis were done with the statistical environment R v. 4.1.1 (R Core Team, 2021).

2.2. Geometric morphometric analyses

The shape affinities of KNM-BG 40021 were explored using a landmark protocol specifically designed to capture the most informative aspects of shape preserved in this specimen (Fig. 2; for further details see SOM S1 and Table S3). We performed a generalized Procrustes analysis (GPA) with the 'Morpho' v. 2.8 package (Schlager, 2017) in R (R Core Team, 2021). We applied semilandmark sliding (identified with SMvector; Schlager, 2017) on curves defined by adjacent landmarks and identified with the function 'outline' (Schlager, 2017). To identify major patterns of shape variation across the sample, we performed a between-group principal component analysis (bgPCA; Mitteroecker and Bookstein, 2011) on the GPA-transformed coordinates of the extant sample, with major anthropoid clades (platyrrhines, cercopithecines, colobines, hylobatids, and hominids) as the grouping factor. To rule out the presence of spurious groupings in the sample, we computed a cross-validated bgPCA and compared the results to those of the bgPCA without cross-validation (Bookstein, 2019; Cardini et al., 2019; Cardini and Polly, 2020). We computed the Z scores and r^2 for group differences in the raw shape data (Adams and Collyer, 2016), and the scores of both the non-cross-validated and the cross-validated bgPCAs using the 'RRPP' v. 2.5 R package (Collyer and Adams, 2018; SOM S1). The fossils were left ungrouped and plotted a posteriori onto the morphospace identified by the bgPCA based on extant taxa. To assess the affinities of each fossil specimen with the a priori defined groups we computed the squared Mahalanobis distances between each individual and the group means using the D2.dist function of the 'biotools' v. 4.2 (Da Silva, 2020) R package, as well as their typicality probabilities using the function typprobClass in 'Morpho' (Table 1; SOM S1). To visualize shape changes occurring along the bgPC axes, we identified the extreme landmark conformations for each bgPC and then warped the 3D model of the individual closest to the mean configuration of the sample—identified with the function 'FindMeanSpec' within 'geomorph' v. 3.1.1 R package (Adams et al., 2020)—toward the obtained configurations. We finally computed an unweighted pair group methods with arithmetic mean (UPGMA) cluster analysis (SOM S1).

To assess correlations between size and shape, ordinary least squares (OLS) and phylogenetic generalized least squares (PGLS; Adams, 2014) regressions of bgPC scores vs. log-transformed centroid size (CS; with natural logarithms, ln CS) were computed using the 'geomorph' v. 3.1.1 R package (Adams et al., 2020). To compute the PGLS regressions, we used a time-calibrated phylogenetic tree based on molecular data downloaded from 10kTrees website v. 3 (Arnold et al., 2010; SOM S1). To evaluate the influence of phylogeny vs. function on the proximal radial shape among extant anthropoids, phylogenetic signal was also quantified by means of both Pagel's λ and Blomberg's K statistics (Pagel, 1999; Blomberg et al., 2003; see SOM S1 for further details) using the 'phytools' v. 0.6-60 R package (Revell, 2012).

3. Results

The bgPCA (Fig. 3) discriminates among extant hominids, hylobatids, and monkeys and correctly classifies 80.2% of cases in the five groups defined a priori (platyrrhines, cercopithecines, colobines, hylobatids, and hominids), while the bgPCA with cross-validation (SOM Fig. S1) correctly classifies 72.4% of cases (SOM S1; SOM Tables S4 and S5). Misclassification cases occur mainly among monkeys, whereas hylobatids are correctly classified in 76% of the cases and hominids in 86% (cross-validated bgPCA; SOM Table S5).

There is no perceptible change between the bgPCA (Fig. 3) and the cross-validated bgPCA (SOM Fig. S1) plots, and the Z-scores are similar for the raw data (6.9), bgPCA (8.7), and cross-validated bgPCA (8.7), implying a similar strength of morphological integration in the datasets. Similarly, r^2 increases from the raw data comparisons (0.26) to both standard (0.52) and cross-validated (0.52) bgPCAs. This indicates that grouping structure is not spurious because there is a comparable increase in r^2 from the raw data to both the standard and cross-validated bgPCAs. Only bgPC1 and bgPC2 (which account for 90% of the variance) are discussed below because bgPC3 (7% variance) and bgPC4 (3% variance) yielded no meaningful patterns.

The bgPC1 (78% of variance) embeds significant but low phylogenetic signal ($K = 0.35$, $p = 0.027$; $\lambda = 0.54$, $p = 0.016$), suggesting a considerable amount of homoplasy, best illustrated by the overlap between *Ateles* and hominids—see SOM S1 for the different implications of K and λ. Although bgPC1 is significantly correlated with ln CS (OLS: $p <$

0.001; PGLS: $p = 0.008$), size only accounts for a small amount of shape variation (OLS: $r^2 = 0.10$ and adjusted $r^2 = 0.09$; PGLS: $r^2 = 0.26$ and adjusted $r^2 = 0.23$). This axis discriminates between hominoids (hominids and hylobatids, overlapping toward negative scores) and cercopithecoids and platyrrhines (which mostly display positive scores, particularly colobines)—except for *Ateles*, which mostly overlaps with hominoids (Fig. 3). *Nacholapithecus* displays slightly positive scores within the hominid variation range, whereas all the other fossils, including *Ekembo* and *Equatorius*, fall within the cercopithecoid–platyrrhine distribution (albeit occupying different positions along bgPC1) apart from hominoids. *Simiolus* displays the most positive scores and *Ekembo* is closer to hominoids (but well distinct from *Nacholapithecus*) among the remaining fossil sample. Shape differences along bgPC1 are driven by the shape of the radial head (Fig. 3) and the mediolateral tilting of the head. Stem catarrhines and monkeys other than *Ateles* (more positive scores) display a more elliptic radial head in proximal view and a medial elevation of the head in anterior view, which results into a mediolateral tilting of the head. In contrast, extant hominoids and *Ateles* (more negative scores) have rounder heads that are not tilted (Fig. 3).

bgPC2 (12% of variance) embeds no significant phylogenetic signal ($K = 0.22$, $p = 0.312$; $\lambda < 0.001$, $p = 1.000$) and is not correlated with ln CS (OLS: $p = 0.083$; PGLS: $p = 0.274$). bgPC2 distinguishes between hominids (positive and slightly negative scores) and hylobatids (more negative scores) with some overlap, but both groups largely overlap with cercopithecoids and platyrrhines, which are not distinguished along this axis (Fig. 3). All the fossils analyzed cluster close to one another, with *Nacholapithecus*, *Ekembo*, and *Dendropithecus* displaying scores closer to 0, and *Simiolus* and *Equatorius* displaying slightly negative scores. Shape differences along bgPC2 are also driven by tilting of the head toward more positive scores. More subtle differences include a more uniformly expanded distal surface area of the radial head toward positive scores, whereas in specimens with more negative scores the distally expanded surface area is more restricted to the anteromedial aspect of the head.

Based on the typicality probabilities for the fossils (Table 1), *Nacholapithecus* is classified as a platyrrhine as first option and as a hominid as second option. *Ekembo*, *Equatorius*, and *Dendropithecus* are also classified as platyrrhines, whereas *Epipliopithecus* and the two *Simiolus* specimens are classified as cercopithecines. The UPGMA analysis clusters *Nacholapithecus* with a subcluster including all extant hominoids (SOM S2; SOM Fig. S2).

4. Discussion and conclusions

We used a landmark protocol that characterizes the anterior aspect of the radial head to analyze the single proximal radial fragment available for *Nacholapithecus*. The overall results are similar to those previously found using a protocol with a more complete proximal radius coverage (Arias-Martorell et al., 2021) but have more limited explanatory power at the morphofunctional level. The shape of the anterior aspect of the radial head is only partially explained by phylogeny, with bgPC2 showing no meaningful phylogenetic signal (as the monkey variation encompasses that of extant hominoids) and bgPC1 displaying significant but low values. The latter denote homoplasy, which might be explained by *Ateles* partially overlapping with hominids due to its convergently evolved hominoid-like humeroradial joint shape (Larson, 1998; Arias-Martorell et al., 2021). Similarities include a round radial head and a more uniform surface area in the distal expansion of the radial head (not circumscribed to the anteromedial side) than in other monkeys (Arias-Martorell et al., 2021).

Functional inferences for the elbow complex of *Nacholapithecus* have been based mostly on the forelimb evidence from the holotype (KNM-BG 35250; Ishida et al., 2004; Nakatsukasa and Kunimatsu, 2009; Takano et al., 2018). The modern hominoid-like globular capitulum of the humerus (KNM-BG 35250M) indicates enhanced mobility at the humeroradial joint and suggests enhanced forearm pronosupination capabilities because of the inferred rounder radial head compared with cercopithecids and stem Miocene hominoids (Takano et al., 2018). As indicated by our shape analysis, *Nacholapithecus* possesses a fairly circular radial head outline with limited tilting and a distal articular surface uniformly expanded to some extent beyond the anteromedial aspect of the radial head. On the morphospace, KNM-BG 40021 displays an intermediate position between extant hominoids and monkeys, close to hominids and overlapping with *Ateles*. This is further supported by the fact that the analysis classifies *Nacholapithecus* as a platyrrhine (first option, owing to its similarities to *Ateles*) or as a hominid (second option).

The anterior aspect of the radial head articulates with the zona conoidea of the humerus in extant apes, whose humeroradial joint is stable throughout all ranges of pronosupination and flexion–extension (Rose, 1988). In contrast, cercopithecoids, have a stable elbow in fully pronated position, where the humeroantebrachial joint achieves a close-packing position (Harrison 1987; Rose, 1988, 1993; Alba et al., 2011). The more extant hominoid-like and atelid-like anterior aspect of the radial head of *Nacholapithecus* is consistent with a radial head that is able to articulate with both the humerus and the ulna in pronated and semipronated forearm positions due to incipient beveling of the radial head beyond the lateral lip (Rose et al., 1992; Takano et al., 2018, 2020)—achieved, in *Nacholapithecus*, by a rounder head and a more uniform distal expansion of the articular area of the radial head than in cercopithecoids, nonsuspensory platyrrhines, and both earlier and coeval Miocene apes. Relative to extant hominoids, *Nacholapithecus* displays a more primitive humeroulnar joint that is not capable of full extension due to a long olecranon process (Takano et al., 2020) and further retains primitive traits at the wrist joint (e.g., ulnocarpal articulation; Ogihara et al., 2016). However, these plesiomorphic features are combined with a humeroradial joint somewhat derived toward the extant hominoid condition than that of early hominoids such as *Ekembo* and *Equatorius* (Takano et al., 2018, 2020). The enhanced stability in wider ranges of pronosupination (especially in semipronated arm positions) of the radiohumeral joint indicated by our results is concordant with previous locomotor inferences for *Nacholapithecus*. Its locomotor repertoire has been described as including forelimb-dominated arboreal behaviors with the forelimbs playing an important role in both body support and overhead positions (Takano et al., 2018, 2020)—i.e., vertical climbing, orthograde clambering, transferring, and bridging in higher frequencies than in Early Miocene apes (e.g., *Ekembo*)—combined with powerful grasping abilities (Ishida et al., 2004; Nakatuskasa et al., 2002, 2007a, 2007b, 2012, 2016; Nakatsukasa and Kunimatsu, 2009; Alba et al., 2011; Ogihara et al., 2016; Ward, 2015; Takano et al., 2018, 2020).

Nevertheless, our results also suggest that the anterior aspect of the radius is not sufficient to distinguish well among groups of quadrupedal taxa with radial heads most suited to maintaining stability in a flexed-elbow and fully pronated hand posture (Rose, 1988)—as illustrated by the considerable overlap between cercopithecines, colobines, and platyrrhines. The fact that small-bodied stem catarrhines and the stem hominoids *Ekembo* and *Equatorius* occupy the same region of the morphospace indicates similarities in the anterior aspect of the radial head, especially in the distal expansion of its articular surface area. This is not surprising given that a more distally expanded anteromedial articular surface area is part of the ancestral anthropoid morphotype (Rose, 1988, 1993, 1994, 1997; Senut, 1989). In previous analyses based on the proximal radius (Arias-Martorell et al., 2021), *Ekembo* and *Equatorius* displayed a clearly intermediate morphology between extant hominoids and monkeys, rather than closer affinities with monkeys. In our bgPCA plot, *Ekembo* is somewhat closer to extant hominoids than *Equatorius* along bgPC1—consistent with differences in their positional behavior (Ward, 1993, 2015; Ward et al., 1993, 1999; McCrossin et al., 1998; Patel et al., 2009)—albeit less so than *Nacholapithecus*, whose humeroradial joint appears more derived toward the crown hominoid condition (Takano et al., 2018, 2020). Small-bodied stem catarrhines display the radial head morphology characteristic of non-hominoid anthropoids and our results broadly agree with those previously obtained (Arias-Martorell et al., 2021) albeit with lower resolution, especially for taxa with a high quadrupedal component.

The mosaic configuration of the elbow joint of *Nacholapithecus*, combining a primitive humeroulnar joint with a quite derived humeroradial joint, supports a stepwise evolution of the anthropoid elbow (Alba et al., 2011, 2015), with extant cercopithecoids and hominoids displaying features derived in opposite directions and stem hominoids displaying mosaic morphologies unlike those of living apes (Alba et al., 2011; Arias-Martorell et al., 2021). The uncertain phylogenetic relationships of *Nacholapithecus* (e.g., Almécija et al., 2021; Urciuoli et al., 2021) hinder to some extent the evolutionary implications of its proximal radial morphology. Nevertheless, the proximal radial morphology of *Nacholapithecus*, more derived than that of *Ekembo* but more primitive than that of crown hominoids, likely reflects an enhancement of pronosupination movements associated with an emphasis on orthograde positional behaviors—compatible with both the stem hominoid (Pugh, 2022) and stem hominid (Alba, 2012; Kunimatsu et al., 2019; Morimoto et al., 2020) status proposed for this taxon. Regardless of its systematic position, the elbow morphology of *Nacholapithecus* suggests that the last common ancestor of crown hominoids displayed a humeroradial joint more primitive than extant hominoids—indicating that the humeroantebrachial complex would have evolved to some extent independently between hylobatids and hominids. The latter notion would be consistent with the independent evolution of orthogrady-related features in atelids and various lineages of crown hominoids (Larson, 1998; Alba, 2012; Almécija et al., 2021) and is further reinforced by the retention of primitive features (likely related to above-branch quadrupedalism) in the humeroulnar joint of the Late Miocene great ape *Hispanopithecus*—recovered as a stem hominid by cladistic analyses (Alba et al., 2015; Pugh, 2022)—despite indicating an elbow complex suitable for preserving stability along the full range of flexion/extension and enabling a broad range of pronosupination as in extant hominoids (Alba et al., 2012).

References

Adams, D.C., 2014. A method for assessing phylogenetic least squares models for shape and other high-dimensional multivariate data. Evolution 68, 2675–2688.

Adams, D.C., Collyer, M.L. 2016. On the comparison of the strength of morphological integration across morphometric datasets. Evolution 70, 2623–2631.

Adams, D.C., Collyer, M.L., Kaliontzopoulou, A., 2020. Geomorph: Software for geometric morphometric analyses. R package version 3.2.1. https://cran.r-project.org/package=geomorph.

Alba, D.M., 2012. Fossil apes from the Vallès-Penedès Basin. Evol. Anthropol. 21, 254–269.

Alba, D.M., Almécija, S., DeMiguel, D., Fortuny, J., Pérez de los Ríos, M., Pina, M., Robles, J.M., Moyà-Solà, S., 2015. Miocene small-bodied ape from Eurasia sheds light on hominoid evolution. Science 350, aab2625.

Almécija, S., Hammond, A.S., Thompson, N.E., Pugh, K.D., Moyà-Solà, S. Alba, D.M. 2021. Fossil apes and human evolution. Science 372, eabb4363.

Almécija, S., Smaers, J.B. Jungers, W.L. 2015. The evolution of human and ape hand proportions. Nat. Comm. 6, 1–11.

Arias-Martorell, J., Almécija, S., Urciuoli, A., Nakatsukasa, M., Moyà-Solà, S., Alba, D.M. 2021. A proximal radius of *Barberapithecus huerzeleri* from Castell de Barberà: Implications for locomotor diversity among pliopithecoids. J. Hum. Evol. 157, 103032.

Arnold, C., Matthews, L.J., Nunn, C.L., 2010. The 10kTrees website: A new online resource for primate phylogeny. Evol. Anthropol. 19, 114–118.

Blomberg, S.P., Garland, T., Ives, A.R., 2003. Testing for phylogenetic signal in comparative data: behavioral traits are more labile. Evolution 57, 717–745.

Bookstein, F.L., 2019. Pathologies of between-groups principal components analysis in geometric morphometrics. Evol. Biol. 46, 271–302.

Cardini, A., Polly, P.D., 2020. Cross-validated between group PCA scatterplots: A solution to spurious group separation? Evol. Biol. 47, 85–95.

Cardini, A., O'Higgins, P., Rohlf, F.J., 2019. Seeing distinct groups where there are none: Spurious patterns from between-group PCA. Evol. Biol. 46, 303–316.

Collyer, M.L., Adams, D.C. 2018. RRPP: An R package for fitting linear models to high-dimensional data using residual randomization. Methods Ecol. Evol. 9, 1772–1779.

Da Silva, A.R., 2020. On testing for seed sample heterogeneity with the exact probability distribution of the germination count range. Seed Sci. Res. 30, 59-63.

Harrison, T., 1987. The phylogenetic relationships of the early catarrhine primates: A review of the current evidence. J. Hum. Evol. 16, 41–80.

Harrison, T., 2010. Dendropithecoidea, Proconsuloidea, and Hominoidea (Catarrhini, Primates). In: Werdelin, L., Sanders, W.J. (Eds.), Cenozoic Mammals of Africa. University of California Press, Berkeley, pp. 429–469.

Ishida, H., Kunimatsu, Y., Nakatsukasa, M., Nakano, Y. 1999. New hominoid genus from the Middle Miocene of Nachola, Kenya. Anthropol. Sci. 107. 189–191

Ishida, H., Kunimatsu, Y., Takano, T., Nakano, Y., Nakatsukasa, M., 2004. *Nacholapithecus* skeleton from the Middle Miocene of Kenya. J. Hum. Evol. 46, 69–103.

Kikuchi, Y., Nakano, Y., Nakatsukasa, M., Kunimatsu, Y., Shimizu, D., Ogihara, N., Tsujikawa, H., Takano, T., Ishida, H., 2012. Functional morphology and anatomy of cervical vertebrae in *Nacholapithecus kerioi*, a middle Miocene hominoid from Kenya. J. Hum. Evol. 62, 677-695.

Kikuchi, Y., Nakatsukasa, M., Nakano, Y., Kunimatsu, Y., Shimizu, D., Ogihara, N., Tsujikawa, H., Takano, T., Ishida, H., 2015. Morphology of the thoracolumbar spine of the middle Miocene hominoid *Nacholapithecus kerioi* from northern Kenya. J. Hum. Evol. 88, 25-42.

Kikuchi, Y., Nakatsukasa, M., Nakano, Y., Kunimatsu, Y., Shimizu, D., Ogihara, N., Tsujikawa, H., Takano, T., Ishida, H., 2016. Sacral vertebral remains of the Middle Miocene hominoid *Nacholapithecus kerioi* from northern Kenya. J. Hum. Evol. 94, 117-125.

Kunimatsu, Y., Nakatsukasa, M., Shimizu, D., Nakano, Y. and Ishida, H. 2019. Loss of the subarcuate fossa and the phylogeny of *Nacholapithecus*. J. Hum. Evol. 131, 22–7.

Larson, S.G., 1998. Parallel evolution in the hominoid trunk and forelimb. Evol. Anthropol. 6, 87–99.

Le Gros Clark, W.E., Thomas, D.P., 1951. Associated jaws and limb bones of *Limnopithecus macinnesi*. Fossil Mammals Afr. 3, 1–27.

McCrossin, L.M., Benefit, B.R., Giteu, S.N., Palmer, A.K., Blue, K.T., 1998. Fossil evidence for the origins of terrestriality among Old World higher primates. In: Strasser, E., Fleagle, J., Rosenberger, A., McHenry, H. (Eds.), Primate Locomotion: Recent Advances. Plenum Press, New York, pp. 353–396.

McNulty, K.P., Begun, D.R., Kelley, J., Manthi, F.K., Mbua, E.N., 2015. A systematic revision of *Proconsul* with the description of a new genus of early Miocene hominoid. J. Hum. Evol. 84, 42–61.

Mitteroecker, P., Bookstein, F., 2011. Linear discrimination, ordination, and the visualization of selection gradients in modern morphometrics. Evol. Biol. 38, 100–114.

Morimoto, N., Kunimatsu, Y., Nakatsukasa, M., Ponce de Leon, M.S., Zollikofer, C.P., Ishida, H., Sasaki, T. Suwa, G. 2020. Variation of bony labyrinthine morphology in Mio−Plio−Pleistocene and modern anthropoids. Am. J. Phys. Anthropol. 173, 276–292.

Nakatsukasa, M., Kunimatsu, Y. 2009. *Nacholapithecus* and its importance for understanding hominoid evolution. Evol. Anthropol. 18, 103–119.

Nakatsukasa, M., Yamanaka, A., Kunimatsu, Y., Shimizu, D., Ishida, H. 1998. A newly discovered *Kenyapithecus* skeleton and its implications for the evolution of positional behavior in Miocene East African hominoids. J. Hum. Evol. 34, 657–664.

Nakatsukasa, M., Kunimatsu, Y., Nakano, Y., Ishida, H. 2002. Morphology of hallucial phalanges in extant anthropoids and fossil hominoids. Z. Morphol. Anthropol. 83, 361–372.

Nakatsukasa, M., Kunimatsu, Y., Nakano, Y., Takano, T., Ishida, H. 2003a. Comparative and functional anatomy of phalanges in *Nacholapithecus kerioi*, a Middle Miocene hominoid from northern Kenya. Primates 44, 371–412.

Nakatsukasa, M., Tsujikawa, H., Shimizu, D., Takano, T., Kunimatsu, Y., Nakano, Y., Ishida H. 2003b. Definitive evidence for tail loss in *Nacholapithecus*, and East African Miocene hominoid. J. Hum. Evol. 45, 179–186.

Nakatsukasa, M., Kunimatsu, Y., Nakano, Y., Ishida, H. 2007a. Vertebral morphology of *Nacholapithecus kerioi* based on KNM-BG 35250. J. Hum. Evol. 52, 347–369.

Nakatsukasa, M., Kunimatsu, Y., Nakano, Y., Egi, N., Ishida, H. 2007b. Postcranial bones of infant *Nacholapithecus*: ontogeny and positional behavioral adaptation. Anthropol. Sci. 115, 201-213.

Nakatsukasa, M., Kunimatsu, Y., Shimizu, D., Nakano, Y., Kikuchi, Y., Ishida, H. 2012. Hind limb of the *Nacholapithecus kerioi* holotype and implications for its positional behavior. Anthropol. Sci. 120, 12073.

Nakatsukasa, M., Almécija, S., Begun, D.R. 2016. The hands of Miocene hominoids. In: Kivell, T.L., Lemelin, P., Richmond, B.G., Schmitt, D. (Eds.), The evolution of the primate hand. Springer, New York, pp. 485–514.

Kunimatsu, Y., Nakatsukasa, M., Shimizu, D., Nakano, Y., Ishida, H., 2019. Loss of the subarcuate fossa and the phylogeny of *Nacholapithecus*. J. Hum. Evol. 131, 22–27.

Ogihara, N., Almécija, S., Nakatsukasa, M., Nakano, Y., Kikuchi, Y., Kunimatsu, Y., Makishima, H., Shimizu, D., Takano, T., Tsujikawa, H., Kagaya, M., Ishida, H. 2016. Carpal bones of *Nacholapithecus kerioi*, a Middle Miocene hominoid from Northern Kenya. Am. J. Phys. Anthropol. 160, 469–482.

Pagel, M., 1999. Inferring the historical patterns of biological evolution. Nature 401, 877–884.

Patel, B.A., 2005. The hominoid proximal radius: Re-interpreting locomotor behaviors in early hominins. J. Hum. Evol. 48, 415–432.

Pina, M., Kikuchi, Y., Nakatsukasa, M., Nakano, Y., Kunimatsu, Y., Ogihara, N., Shimizu, D., Takano, T., Tsujikawa, H., Ishida, H., 2021. New femoral remains of *Nacholapithecus kerioi*: Implications for intraspecific variation and Miocene hominoid evolution. J. Hum. Evol. 155, 102982.

Pugh, K.D. 2022. Phylogenetic analysis of Middle-Late Miocene apes. J. Hum. Evol. 165, 103140.

R Core Team, 2021. R: A language and environment for statistical computing. R Foundation for Statistical Computing, Vienna.

Revell, L.J., 2012. Phytools: An R package for phylogenetic comparative biology (and other things). Methods Ecol. Evol. 3, 217–223.

Rose, M.D., 1988. Another look at the anthropoid elbow. J. Hum. Evol. 17, 193–224.

Rose, M.D., 1993. Locomotor anatomy of Miocene hominoids. In: Gebo, D.L. (Ed.), Postcranial Adaptation in Nonhuman Primates. Northern Illinois University Press, DeKalb, pp. 252–272.

Rose, M.D., 1994. Quadrupedalism in some Miocene catarrhines. J. Hum. Evol. 26, 387–411.

Rose, M.D., 1997. Functional and phylogenetic features of the forelimb in Miocene hominoids. In: Begun, D.R., Ward, C.V., Rose, M.D. (Eds.), Function, Phylogeny and Fossils: Miocene Hominoid Evolution and Adaptation. Plenum Press, New York, pp. 79–100.

Rose, M.D., Leakey, M.G., Leakey, R.E.F., Walker, A.C., 1992. Postcranial specimens of *Simiolus enjiessi* and other primitive catarrhines from the early Miocene of Lake Turkana, Kenya. J. Hum. Evol. 22, 171–237.

Rose, M.D., Nakano, Y., Ishida, H. 1996. *Kenyapithecus* postcranial specimens from Nachola, Kenya. Afr. Study Monogr. 24, 3–56.

Rossie, J.B., Gutierrez, M., Goble, E., 2012. Fossil forelimbs of *Simiolus* from Moruorot, Kenya. Am. J. Phys. Anthropol. 147 (S54), 252.

Ruff, C.B., 2002. Long bone articular and diaphyseal structure in Old World monkeys and apes. I: Locomotor effects. Am. J. Phys. Anthropol. 119, 305–342.

Ruff, C.B., 2003. Long bone articular and diaphyseal structure in Old World monkeys and apes. II: Estimation of body mass. Am. J. Phys. Anthropol. 120, 16–37.

Sawada, Y., Pickford, M., Itaya, T., Makinouchi, T., Tateishi, M., Kabeto, K., Ishida, S., Ishida, H., 1998. K-Ar ages of Miocene Hominoidea (*Kenyapithecus* and *Samburupithecus*) from Samburu Hills, Northern Kenya. C. R. Acad. Sci. Paris 326, 445–451.

Sawada, Y., Saneyoshi, M., Nakayama, K., Sakai, T., Itaya, T., Hyodo, M., Mukokya, Y., Pickford, M., Senut, B., Tanaka, S., Chujo, T., Ishida, H. 2006. The ages and geological background of Miocene hominoids *Nacholapithecus*, *Samburupithecus*, and *Orrorin* from Kenya. In: H. Ishida, R. Tuttle, M. Pickford, N. Ogihara, M. Nakatsukasa (Eds.), Human origins and environmental backgrounds. Developments in Primatology: Progress and Prospects. Springer, New York, pp. 71-96

Schlager, S., 2017. Morpho and Rvcg – shape analysis in R: R-packages for geometric morphometrics, shape analysis and surface manipulations. In: Zheng, G., Li, S., Székely, G. (Eds.), Statistical Shape and Deformation Analysis. Methods, Implementation and Applications. Academic Press, London, pp. 217–256.

Senut, B., 1989. Le Coude des Primates Hominoïdes. Anatomie, Fonction, Taxonomie, Évolution. Éditions du Centre National de la Recerche Scientifique, Paris.

Senut, B., Nakatsukasa, M., Kunimatsu, Y., Nakano, Y., Takano, T., Tsujikawa, H., Shimizu, D., Kagaya, M., Ishida, H. 2004. Preliminary analysis of *Nacholapithecus* scapula and clavicle from Nachola, Kenya. Primates 45, 97-104.

Sherwood, R.J., Ward, R.J., Hill, A., Duren, D.L., Brown, B., Downs, W., 2002. Preliminary description of the *Equatorius africanus* partial skeleton KNM-TH 28860 from Kipsaramon, Tugen Hills, Baringo District, Kenya. J. Hum. Evol. 42, 63–73.

Takano, T., Nakatsukasa, M., Kunimatsu, Y., Nakano, N., Ogihara N., Ishida, H. 2018. Forelimb long bones of *Nacholapithecus* (KNM-BG 35250) from the middle Miocene in Nachola, northern Kenya. Anthropol. Sci. 126, 135–149.

Takano, T., Nakatsukasa, M., Pina, M., Kunimatsu, Y., Nakano, Y., Morimoto, N., Ogihara, N., Ishida, H. 2020. New forelimb long bone specimens of *Nacholapithecus kerioi* from the Middle Miocene of northern Kenya. Anthropol. Sci. 128, 200116.

Urciuoli, A., Zanolli, C., Almecija, S., Alba, D.M. 2020. Reassessment of the phylogenetic relationships of the late Miocene apes *Hispanopithecus* and *Rudapithecus* based on vertibular morphology. Proc. Natl. Acad. Sci. USA 118, e2015215118.

Walker, A.C., Pickford, M., 1983. New postcranial fossils of *Proconsul africanus* and *Proconsul nyanzae*. In: Ciochon, R.L., Corruccini, R.S. (Eds.), New Interpretations of Ape and Human Ancestry. Plenum Press, New York, pp. 325–351.

Ward, C.V., 1993. Torso morphology and locomotion in *Proconsul nyanzae*. Am. J. Phys. Anthropol. 92, 291–328.

Ward, C.V., 2015. Postcranial and locomotor adaptations of hominoids. In: Henke, W., Tattersall, I. (Eds.), Handbook of Paleoanthropology, 2nd ed. Springer, Heidelberg, pp. 1363–1386.

Ward, C.V., Walker, A., Teaford, M.F., Odhiambo, L., 1993. Partial skeleton of *Proconsul nyanzae* from Mfangano Island, Kenya. Am. J. Phys. Anthropol. 90, 77–111.

Ward, S., Brown, B., Hill, A., Kelley, J., Downs, W., 1999. *Equatorius*: A new hominoid genus from the middle Miocene of Kenya. Science 285, 1382–1386.

Wiley, D.F., Amenta, N., Alcantara, D.A., Ghosh, D., Kil, Y.J., Delson, E., Harcourt-Smith, W., Rohlf, F.J., St John, K., Hamann, B., 2005. Evolutionary morphing. In: Silva, T.C., Gorller, E., Rushmeier, H. (Eds.), VIS 05 IEEE Visualization. IEEE, Minneapolis, pp. 431–438.

Zapfe, H., 1958. The skeleton of *Pliopithecus (Epipliopithecus) vindobonensis* Zapfe and Hürzeler. Am. J. Phys. Anthropol. 16, 441–457.

Zapfe, H., 1961. Die Primatenfunde aus der miozänen Spaltenfüllung von Neudorf an der March (Děvínská Nová Ves), Tschechoslowakei. Schweizer. Palaeontol. Abh. 78, 1–293.

Figure captions

Figure 1. Right proximal radial fragment (KNM BG 40021) of *Nacholapithecus kerioi* from the Aka Aiteputh Formation in Nachola, Kenya, in proximal (a), anterior (b), and medial (c) views.

Figure 2. Landmark protocol illustrated on renderings of a 3D model of the right proximal radial fragment (KNM-BG 40021, mirrored) of *Nacholapithecus kerioi*, in proximal (a), anterior (b), lateral (c), and medial (d) views. Landmarks (L, bolded) and semilandmarks (SL) are denoted by black and red dots, respectively, and described in SOM Table S3.

Figure 3. Results of the between-group principal component analysis as depicted by a bivariate plot of bgPC2 vs. bgPC1. Groups distinguished a priori are denoted by color coded convex hulls and symbols: violet = hominids; green = hylobatids; orange = cercopithecines; emerald = colobines; pink = platyrrhines. Extant genera are denoted by different symbols (see legend). The scatter of *Ateles* is highlighted with a convex hull in darker pink within the

platyrrhine distribution. Fossil specimens (scores projected a posteriori) are denoted by colored stars (see legend). The percentage of variance explained by each bgPC is reported within parentheses. Renderings along axes represent maximum and minimum shape changes for that axis (corresponding to their position at the positive and negative ends of each axis). Abbreviation: bgPC = between-group principal component.

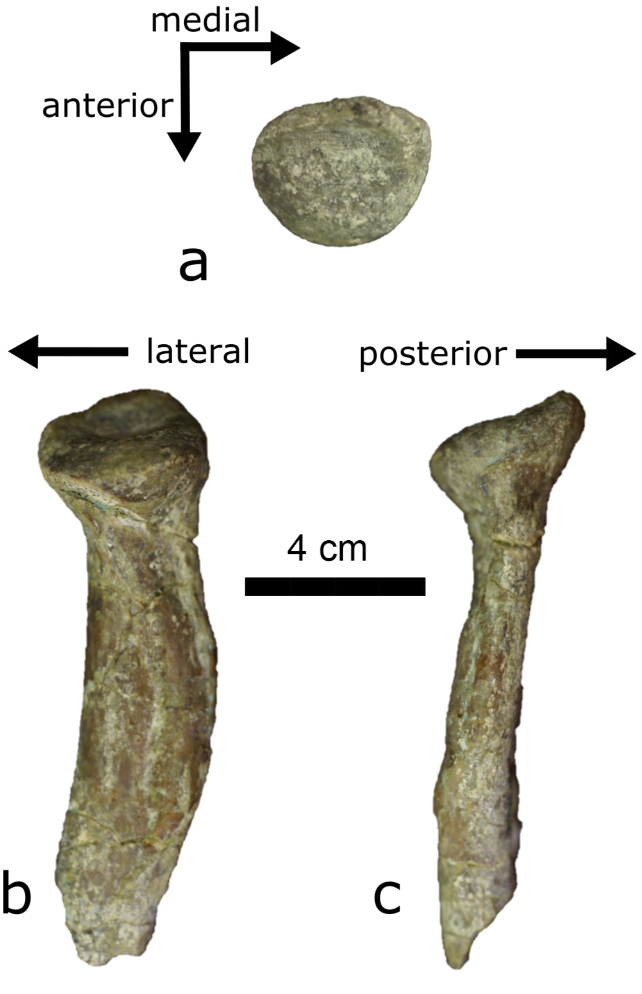
medial
anterior
a
lateral
posterior
4 cm
b
c

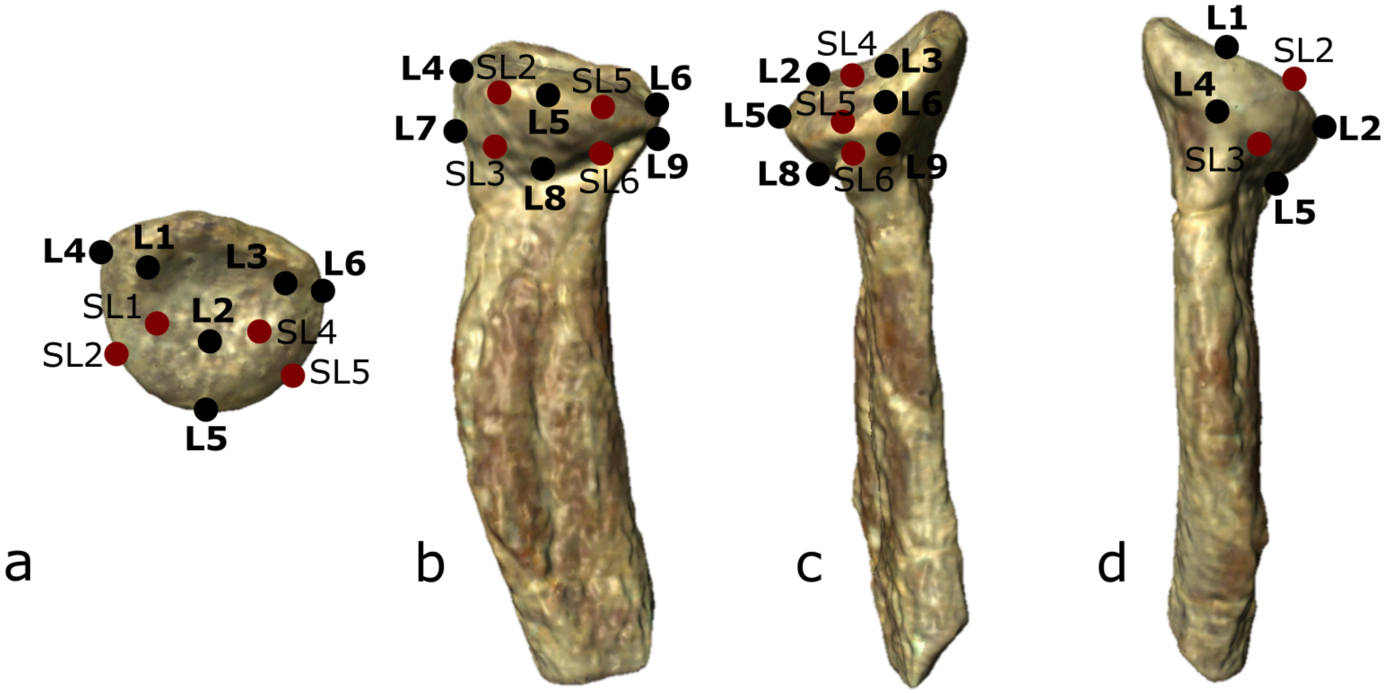
L4
L1
L3
L6
SL1
L2
SL4
SL2
SL5
L5
a
L4
SL2
SL5
L6
L7
L5
L9
SL3
L8
SL6
b
SL4
L2
L3
L5
SL5
L6
L8
SL6
L9
c
L1
SL2
L4
L2
SL3
L5
d

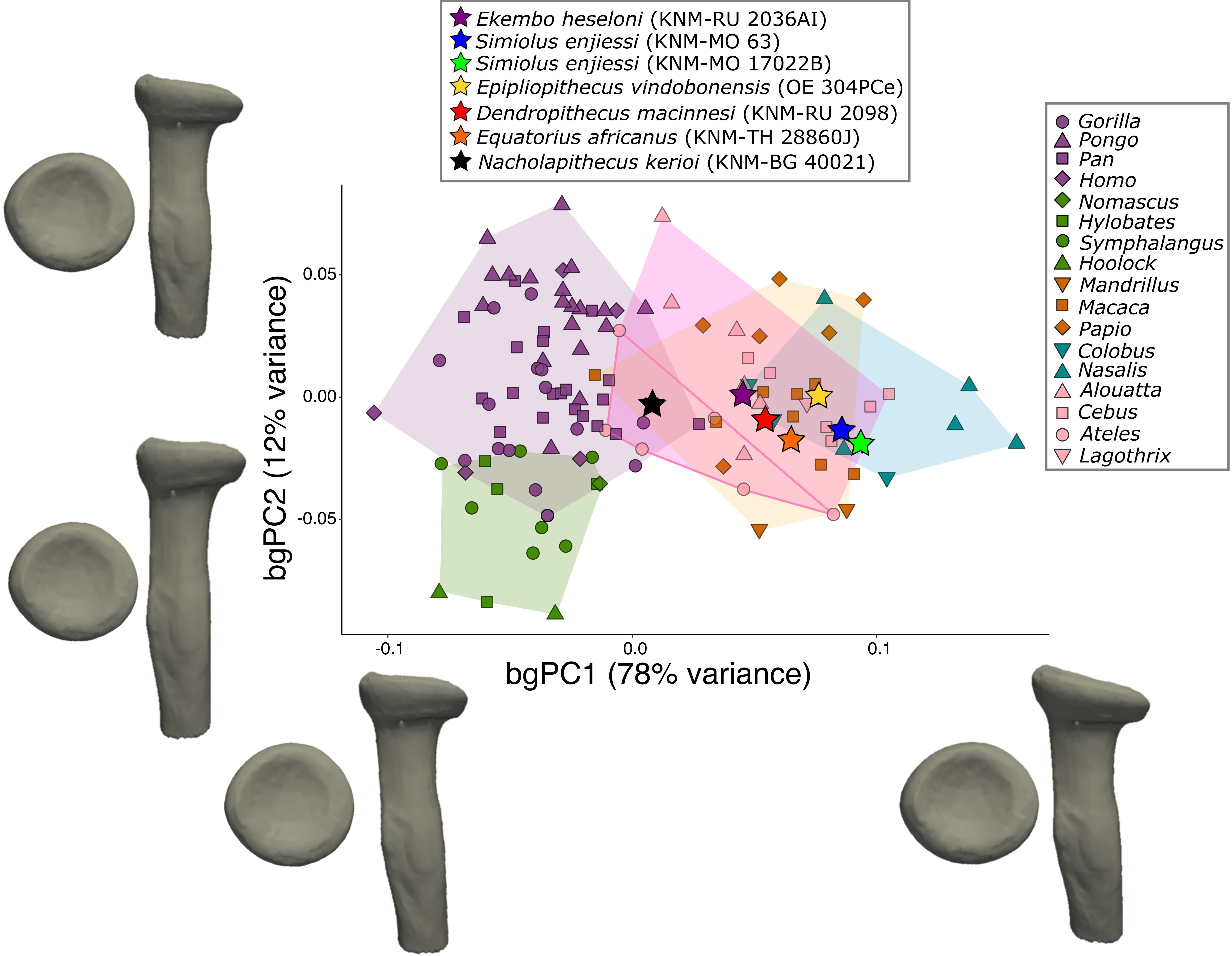

Ekembo heseloni (KNM-RU 2036AI)
Simiolus enjiessi (KNM-MO 63)
Simiolus enjiessi (KNM-MO 17022B)
Epipliopithecus vindobonensis (OE 304PCe)
Dendropithecus macinnesi (KNM-RU 2098)
Equatorius africanus (KNM-TH 28860J)
Nacholapithecus kerioi (KNM-BG 40021)
Gorilla
Pongo
Pan
Homo
Nomascus
Hylobates
Symphalangus
Hoolock
Mandrillus
Macaca
Papio
Colobus
Nasalis
Alouatta
Cebus
Ateles
Lagothrix
bgPC2 (12% variance)
0.05
0.00
-0.05
bgPC1 (78% variance)
-0.1
0.0
0.1

Table 1

Squared Mahalanobis distances (D^2) between fossils and group means, and classification results based on typicality probabilities (p) of the fossils computed from the between-group principal component analysis of radial head shape.[a]

Species	Catalogue No.	D^2/p	Cercopithecines	Colobines	Hominids	Hylobatids	Platyrrhines
Nacholapithecus kerioi	KNM-BG 40021	D^2	9.892	8.325	7.317	6.062	**1.782**
		p	0.014	0.010	0.217*	0.015	**0.486****
Ekembo heseloni	KNM-RU 2036CE	D^2	3.878	5.265	4.770	11.891	**0.603**
		p	0.529*	0.107	0.062	0.002	**0.983****
Equatorius africanus	KNM-TH 28860-J	D^2	4.002	4.385	11.520	7.729	**2.919**
		p	0.689*	0.155	0.007	0.001	**0.827****
Epipliopithecus vindobonensis	O.E. 304 PCe	D^2	7.576	17.238	10.630	16.416	**5.385**
		p	**0.127****	<0.001	<0.001	<0.001	0.056*
Dendropithecus macinnesi	KNM-RU 2098	D^2	15.063	8.5177	12.022	13.748	**1.964**
		p	0.031	0.118*	0.004	<0.001	**0.874****
Simiolus enjiessi	KNM-MO 63	D^2	12.904	12.547	13.622	14.547	**3.052**
		p	**0.528****	0.011	<0.001	<0.001	0.233*

Simiolus enjiessi	KNM-MO 17022B	D^2	**5.533**	11.160	16.496	11.045	6.580
		p	**0.304****	0.003	<0.001	<0.001	0.088*

[a] Group membership was rejected at $p < 0.05$. Two asterisks (**) denote primary group classification; one asterisk (*) denotes secondary group classification. Shortest D^2 and highest p-values are bolded.

Supplementary Online Material (SOM):

The radial head of the Middle Miocene ape *Nacholapithecus kerioi*: Morphometric affinities, locomotor inferences, and implications for the evolution of the hominoid humeroradial joint

SOM S1

Supplementary materials and methods

Scanning

The radii of *Simiolus enjiessi* KNM-RU 17022B and of *Epipliopithecus vindobonensis* O.E. 304 PCe were scanned from high-quality casts housed in the Institut Català de Paleontologia Miquel Crusafont (ICP, Cerdanyola del Vallès, Spain). All the other fossils (see SOM Table S1) were scanned from original specimens at the Kenya National Museums with a NextEngine surface laser scanner (Next Engine, Santa Monica) using the HD3 macro mode. The 3D models of the extant specimens were obtained using a NextEngine surface scanner and two different high-resolution μCT scanners (SOM Table S2): a BIR ACTIS 225/300 industrial μCT scanner (Department of Human Evolution, Max Planck Institute for Evolutionary Anthropology, Germany) and a Nikon XT 225 ST μCT scanner (Cambridge Biotomography Centre, Department of Zoology, University of Cambridge, UK). Specimens scanned with the NextEngine scanner were obtained using a resolution of >10,000 points per square inch; 6–12 scans were taken at two or more positions and then merged using ScanStudio HD PRO software v. 1.3.2 (Next Engine, Santa Monica). The isotropic voxel size range for the μCT scans sample is 21.9–51.5 μm. Laser scan-derived 3D models were cleaned (fill holes, irregularities in mesh, etc.) using Geomagic Wrap 2017 (3D Systems, Inc. Morrisville), and μCT scans were processed in AVIZO v. 6.3 (Visualization Sciences Group, Berlin).

Landmark protocol

Our landmark protocol was specifically devised to capture the shape affinities of KNM-BG 40021. It consists of 15 3D landmarks including 9 type II and 6 semilandmarks (Fig. 2; SOM Table S3). Type II landmarks reflect points in anatomical structures that can be recognized by their geometry, such as the maximum point of a curve. The homology of type III landmarks is given relative to the other landmarks around them, which should be type I or type II (therefore, a type III landmark would be the middle point between two 'true' landmarks, for example; Bookstein, 1997; O'Higgins, 2000). The protocol thus captures the anterior aspect of the radial head, including the anterior outline of the fovea (L1–3, SL1–2), the anterior outline of the radial head (L4–6, SL3–4), and the distal expansion of articular surface (L7–9, SL5–6). Radii were oriented in anterior view, either using anatomical orientation (complete radii) or based on the anteromedial position of the radial tuberosity, which was preserved in all individuals, allowing a swift identification of the medial, lateral, and posterior aspects of the radial head (as type II landmarks depend on correct orientation for placement; Zelditch et al., 2012). All type II landmarks (L1–9) were used in a previous study of the proximal radius of fossil catarrhines (Arias-Martorell et al., 2021). We included six additional semilandmarks to ensure a more detailed and accurate representation of the anterior aspect of the shape of the radial head (Bookstein, 1997). Shape changes occurring along the axes of the bgPCA depicted in Figure 3 were visualized by warping the specimen closest to the mean configuration—identified with the 'findMeanSpec' function in Geomorph (Adams et al., 2020)—toward the extreme landmark configurations for each bgPC.

Statistics

We computed the standard deviates of observed statistics as effect sizes from distributions of random outcomes. We used these to compare the strength of morphological integration across morphometric datasets using the statistic test (Z-score) under the null hypothesis of a random association of variables. The method displays a constant expected value and confidence intervals and thus provides a consistent measure of integration suitable for comparisons across datasets (Adams and Collyer, 2016).

To assess the similarity of a fossil specimen's score to each a priori defined group based on their distribution of scores (variability) we used typicality probabilities. These are computed based on the Mahalanobis square distance (D^2) between the specimen and the group centroids and represent the p-value to test the null hypothesis of group membership. Hence, a specimen is considered an outlier for a given group when $p < 0.05$, while higher typicality probabilities denote closer affinities between the individual and the distribution of the group. Note that the sum of the typicality probabilities for a given specimen does not equal 1, as they do not assume that the specimen must belong to one of the groups defined a priori, and rather represent the likelihood of belonging to each a priori defined group separately. In the UPGMA analysis, we used the mean Procrustes coordinates of each group, of the two *Simiolus* specimens, and the other fossils.

To compute the amount of phylogenetic signal embedded in the shape data we computed both Pagel's λ (Pagel, 1999; Freckleton et al., 2002) and Bloomberg's K (Blomberg et al., 2003) statistics. Both compare the observed data distribution to that expected under a Brownian motion model of evolution but they are not entirely comparable: λ compares the actual covariance among species with that expected under Brownian motion, whereas K more specifically reflects how variance is partitioned. Pagel's λ ranges from 0 to 1: $\lambda = 1$ implies that trait covariance is exclusively influenced by phylogeny, $\lambda < 1$ suggests that other factors besides phylogeny influence trait evolution, and $\lambda = 0$ is obtained when no phylogenetic correlation is found in the data. In contrast, Blomberg's K may vary beyond unity: $K \approx 1$ similarly implies a model of evolution that closely resembles that expected under Brownian motion, $K < 1$ implies that closely related taxa resemble each other less than expected (variance accumulates within clades), possibly because of independent evolution (i.e., homoplasy), and $K > 1$ implies that closely related taxa are more similar than expected, so that variance accumulates among clades (as the result of stabilizing selection or architectural constraints).

SOM S2

Supplementary results

Shape changes were warped onto the specimen of *Pan troglodytes* USNM-220062, which was identified to be the closest to the mean configuration with a Mahalanobis distance of 0.068. In the UPGMA analysis, all the monkeys clustered together, including a subcluster for *Lagothrix*, *Simiolus*, and *Epipliopithecus*, apart from the hominoid + *Nacholapithecus* cluster. *Ekembo* did not cluster with any other taxon but is at the base of the monkey + small fossil catarrhines cluster, whereas *Equatorius* and *Dendropitheus* clustered apart from all the other taxa.

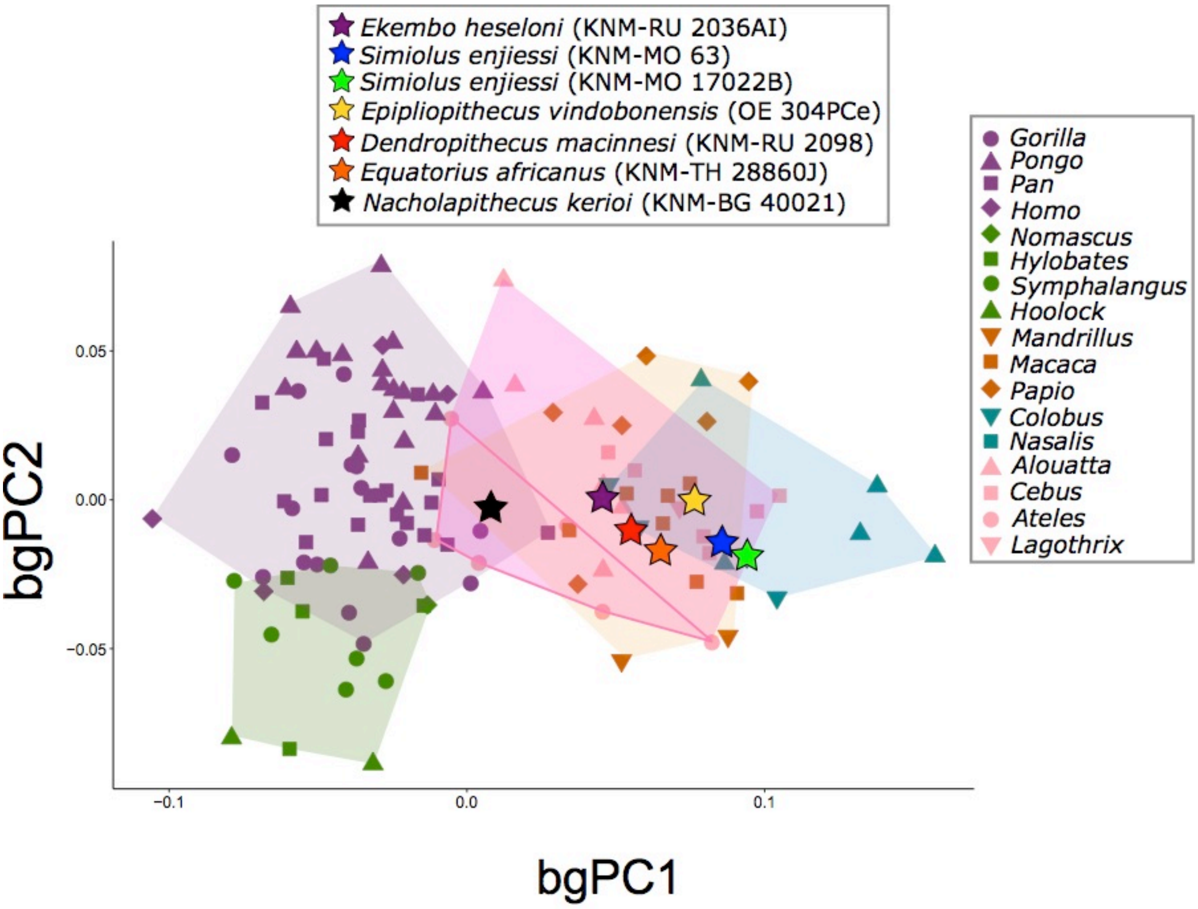

SOM Figure S1. Results of the cross-validated between-group principal component (bgPC) analysis of proximal radial shape among extant anthropoid primates as depicted by a bivariate plot of bgPC2 vs. bgPC1. Groups distinguished a priori are denoted by color-coded convex hulls and symbols: violet = hominids; green = hylobatids; orange = cercopithecines; emerald = colobines; pink = platyrrhines. The scatter of *Ateles* is highlighted with a convex hull in darker pink within the platyrrhine distribution. Extant genera are denoted by different symbols (see legend). Fossil specimens (scores projected a posteriori) are denoted by colored stars (see legend).

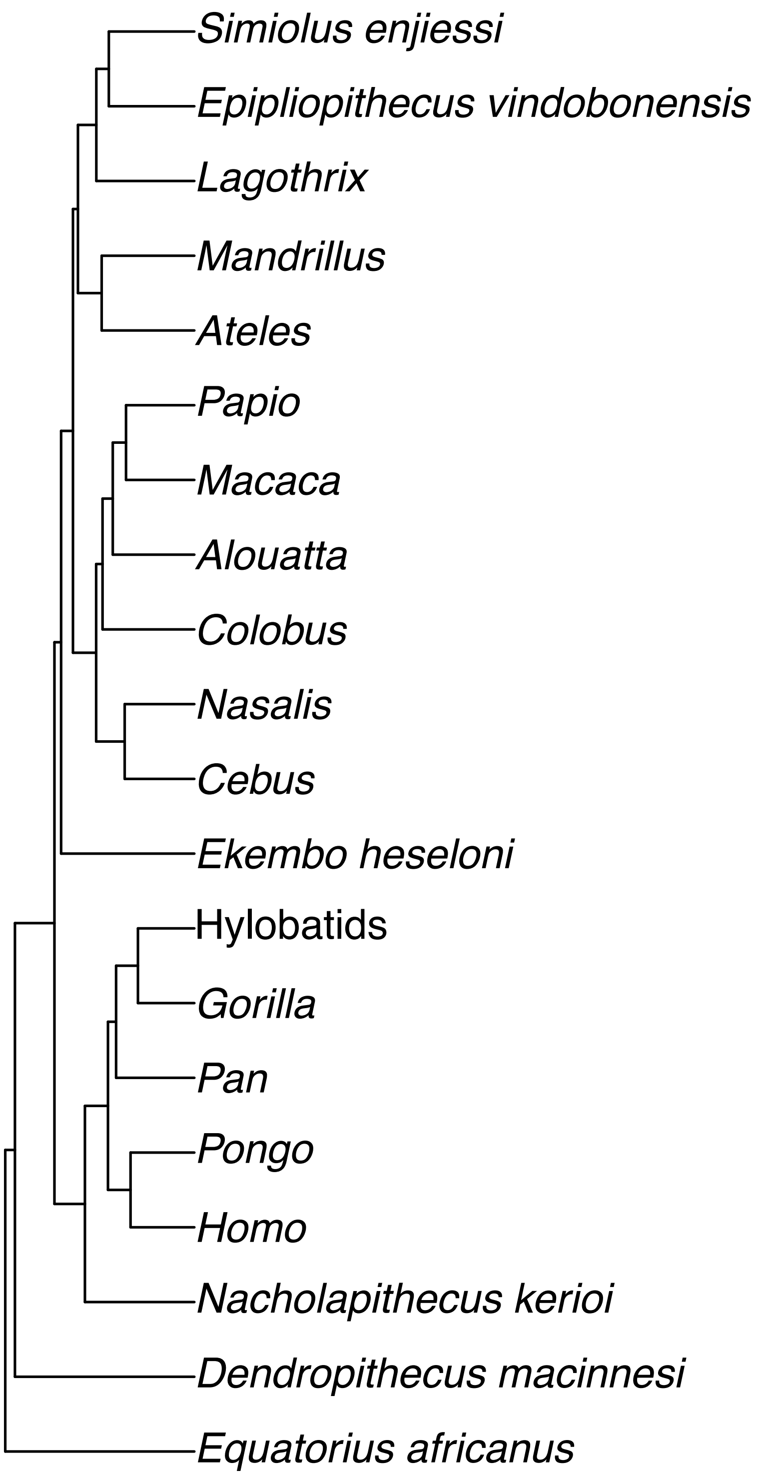

SOM Figure S2. Dendrogram derived from the unweighted pair group methods with arithmetic mean (UPGMA) cluster analysis. Cophenetic correlation was $r^2 = 0.84$.

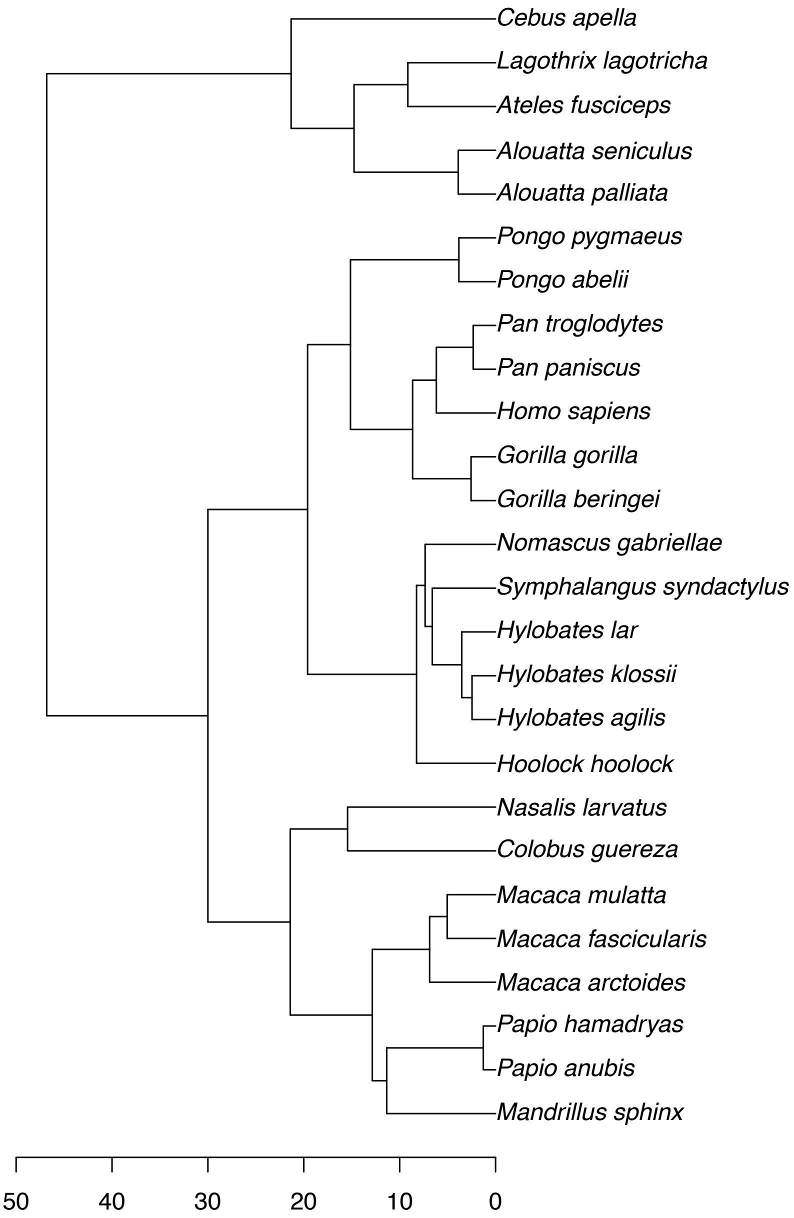

SOM Figure S3. Consensus molecular tree downloaded from 10kTrees website v. 3 (www.10Ktrees.org) used to compute phylogenetic signal and conduct the phylogenetic generalized least squares analyses.

SOM Table S1

Details of the fossil comparative sample.

Species	Catalogue no.	Site	References
Simiolus enjiessi	KNM-MO 63	Moruorot	Rose et al. (1992: Fig. 8); Senut (1989: Fig. 62); Rossie et al. (2012)
Simiolus enjiessi	KNM-MO 17022B	Kalodirr	Rose et al. (1992: Fig. 9)
Dendropithecus macinnesi	KNM-RU 2098	Rusinga Island	Le Gros Clark and Thomas (1951: Pl. 4 Fig. 9, Pl. 5 Fig. 11); Senut (1989: Fig. 76 and Pl. X)
Epipliopithecus vindobonensis	O.E. 304 PCe	Devínska Nová Ves	Zapfe (1958: Pl. 1A and Fig. B5); Zapfe (1961: Fig. 54); Senut (1989: Fig. 95 and Pl. XV)
Ekembo heseloni	KNM-RU 2036CE	Rusinga Island	Walker and Pickford (1983: Fig. 4); Senut, 1989 (Fig. 74 and Pl. VII)
Equatorius africanus	KNM-TH 28860-J	Kipsaraman	Ward et al. (1999: Fig 2k); Sherwood et al. (2002: Fig. 1f)

SOM Table S2

Details of the extant primate sample used in the study. Media and identifier (when available) are listed for specimens downloaded from Morphosource.org.

Species	Catalog no.	Sex	Side	Source	Media	Identifier	Scanner
Alouatta palliata aequatorialis	USNM 338107	M	L	USNM	—	—	NextEngine
Alouatta palliata palliata	USNM 282798	F	L	USNM	—	—	NextEngine
Alouatta seniculus	AMNH 42316	F	L	AMNH	—	—	NextEngine
Alouatta seniculus	AMNH 23333	M	L	AMNH	—	—	NextEngine
Alouatta sp.	ZMB 35764	M	L	ZMB	—	—	µCT (BIR ACTIS)
Alouatta sp.	ZMS 1973-0330	?	R	ZMS	—	—	µCT (BIR ACTIS)
Ateles fusciceps robustus	USNM 338111	F	L	USNM	—	—	NextEngine
Ateles fusciceps robustus	USNM 338112	M	L	USNM	—	—	NextEngine
Ateles sp.	ZMB 45255	F	R	ZMB	—	—	µCT (BIR ACTIS)
Ateles sp.	ZMB 44814	M	R	ZMB	—	—	µCT (BIR ACTIS)
Ateles sp.	ZMB 38734	?	R	ZMB	—	—	µCT (BIR ACTIS)
Ateles sp.	ZMB 44079	?	L	ZMB	—	—	µCT (BIR ACTIS)
Cebus apella apella	USNM 361020	M	L	USNM	—	—	NextEngine
Cebus apella	USNM 397940	F	R	USNM	—	—	NextEngine
Cebus apella	AMNH 133606	M	L	AMNH	—	—	NextEngine
Cebus apella paraguanayanus	AMNH 133631	M	R	MS	M12099-19605	urn:catalog:AMNH:Mammals:M-133631	—
Cebus apella paraguayanus	AMNH 133623	M	R	MS	M12095-19594	urn:catalog:AMNH:Mammals:M-133623	—
Cebus apella paraguayanus	AMNH 133628	M	R	MS	M12093-19588	urn:catalog:AMNH:Mammals:M-133628	—

Colobus guereza	AMNH 52223	F	L	AMNH	—	—	NextEngine
Colobus guereza	AMNH 52241	F	L	AMNH	—	—	NextEngine
Colobus guereza kikuyuensis	USNM 452621	M	L	USNM	—	—	NextEngine
Colobus guereza	AMNH 52248	M	L	AMNH	—	—	NextEngine
Colobus guereza	USNM 452632	F	L	USNM	—	—	NextEngine
Gorilla beringei beringei	AMNH 54091	F	L	AMNH	—	—	NextEngine
Gorilla beringei beringei	RMCA 2263	F	L	RMCA	—	—	NextEngine
Gorilla beringei beringei	USNM 395636	M	L	USNM	—	—	NextEngine
Gorilla beringei beringei	USNM 396934	M	L	Morphosource	M56720-102006	http://n2t.net/ark:/65665/313444cf4-f1e7-4bbc-ba69-039e4d4557e4	—
Gorilla beringei beringei	USNM 396937	F	L	Morphosource	M57009-102295	http://n2t.net/ark:/65665/32f41b8f5-9a15-4f88-af7e-8218ebf0b616	—
Gorilla beringei beringei	USNM 397351	M	L	Morphosource	M56268-101554	http://n2t.net/ark:/65665/3db306794-3c8e-4930-bb20-e514ac62bac6	—
Gorilla beringei graueri	AMNH 202932	M	R	AMNH	—	—	NextEngine
Gorilla beringei graueri	RMCA 8187	M	L	RMCA	—	—	NextEngine
Gorilla beringei	USNM 239883	M	L	USNM	—	—	NextEngine
Gorilla gorilla	USNM 586541	F	R	USNM	—	—	NextEngine
Gorilla gorilla gorilla	AMNH 1673390	F	L	AMNH	—	—	NextEngine
Gorilla gorilla	CMNH 2767	M	L	CMNH	—	—	NextEngine
Gorilla gorilla	USNM 174722	M	R	USNM	—	—	NextEngine
Gorilla gorilla	USNM 176225	M	L	USNM	—	—	NextEngine
Gorilla gorilla	MER 300	F	R	PCM	—	—	µCT (Nikon)
Homo sapiens	AMNH 99-8376	F	L	AMNH	—	—	NextEngine
Homo sapiens	USNM 1512	F	L	USNM	—	—	NextEngine
Homo sapiens	AMNH 20-3501	M	L	AMNH	—	—	NextEngine

Homo sapiens	USNM 942	M	L	USNM	—	—	NextEngine
Homo sapiens	PSU 105-1793	?	L	MS	M45359-82651	—	—
Hoolock hoolock	AMNH 83425	F	R	AMNH	—	—	NextEngine
Hoolock hoolock	AMNH 83420	M	R	AMNH	—	—	NextEngine
Hylobates agilis	AMNH 106575	F	L	AMNH	—	—	NextEngine
Hylobates klossii	AMNH 103344	M	R	AMNH	—	—	NextEngine
Hylobates klossii	AMNH 103347	M	L	AMNH	—	—	NextEngine
Hylobates lar vestitus	NMNH 271047	F	L	USNM	—	—	NextEngine
Lagothrix lagotricha	DU-BAA 90	?	R	MS	M12471-20497	ark:/87602/m4/M20497	—
Macaca arctoides	AMNH 112727	F	L	AMNH	—	—	NextEngine
Macaca fascicularis	USNM 271168	M	R	USNM	—	—	NextEngine
Macaca fascicularis	ZMB 48496	?	L	ZMB	—	—	µCT (BIR ACTIS)
Macaca fascicularis	ZMB 49090	?	L	ZMB	—	—	µCT (BIR ACTIS)
Macaca fascicularis	ZMB 49092	?	L	ZMB	—	—	µCT (BIR ACTIS)
Macaca mulatta	DU-BAA 142	?	R	MS	M12472-20500	—	—
Macaca mulatta	USNM 537241	F	L	USNM	—	—	NextEngine
Macaca mulatta	USNM 537253	M	L	USNM	—	—	NextEngine
Mandrillus sphinx	AMNH 89361	M	R	MS	M10169-14599	urn:catalog:AMNH:Mammals:M-89361	—
Mandrillus sphinx	AMNH 89365	M	R	MS	M10176-14633	urn:catalog:AMNH:Mammals:M-89365	—
Nasalis larvatus	USNM 536050	F	L	USNM	—	—	NextEngine
Nasalis larvatus	AMNH 106275	M	L	AMNH	—	—	NextEngine
Nasalis larvatus	AMNH 198276	M	L	USNM	—	—	NextEngine
Nomascus gabriellae	AMNH 87253	F	L	AMNH	—	—	NextEngine

Pan paniscus	AMNH 86857	F	L	AMNH	—	—	NextEngine
Pan paniscus	RMCA 29045	F	L	RMCA	—	—	NextEngine
Pan paniscus	RMCA 27696	M	R	RMCA	—	—	NextEngine
Pan paniscus	SBU 87-1	M	L	SBU	—	—	NextEngine
Pan troglodytes	USNM 176226	F	L	USNM	—	—	NextEngine
Pan troglodytes	USNM 176229	F	L	USNM	—	—	NextEngine
Pan troglodytes	USNM 176227	M	L	USNM	—	—	NextEngine
Pan troglodytes	USNM 220327	M	L	USNM	—	—	NextEngine
Pan troglodytes	USNM 395820	M	L	USNM	—	—	NextEngine
Pan troglodytes	UNSM 481804	M	R	USNM	—	—	NextEngine
Pan troglodytes schweinfurthii	AMNH 51376	M	R	MS	M10175-14630	urn:catalog:AMNH:Mammals:M-51376	—
Pan troglodytes schweinfurthii	AMNH 51393	M	R	MS	M10242-14814	urn:catalog:AMNH:Mammals:M-51393	—
Pan troglodytes troglodytes	AMNH 54330	M	L	MS	M10240-14808	urn:catalog:AMNH:Mammals:M-54330	—
Pan troglodytes troglodytes	USNM 220064	F	L	USNM	—	—	NextEngine
Pan troglodytes troglodytes	USNM 220062	F	L	MS	M56889-102175	http://n2t.net/ark:/65665/3dcfb7753-f4d7-4334-9b52-6f9f1b9ea03e	—
Pan troglodytes troglodytes	USNM 220063	F	L	MS	M56483-101769	http://n2t.net/ark:/65665/386ed1f25-2f34-459d-91e5-d0111c2e0dc6	—
Pan troglodytes verus	MPI-EVA 11778	F	L	MPI	—	—	µCT (BIR ACTIS)
Pan troglodytes verus	MPI-EVA 13429	F	L	MPI	—	—	µCT (BIR ACTIS)
Pan troglodytes verus	MPI-EVA 15001	F	L	MPI	—	—	µCT (BIR ACTIS)
Pan troglodytes verus	AMNH 89406	M	L	AMNH	—	—	NextEngine
Papio anubis	AMNH 52668	F	L	AMNH	—	—	NextEngine

Papio anubis	AMNH 120388	M	L	AMNH	—	—	NextEngine
Papio anubis neumanni	USNM 384235	F	L	USNM	—	—	NextEngine
Papio anubis neumanni	USNM 384229	M	L	USNM	—	—	NextEngine
Papio hamadryas	ZMB 105450	M	R	ZMB	—	—	µCT (BIR ACTIS)
Papio hamadryas	ZMB 65265	M	L	ZMB	—	—	µCT (BIR ACTIS)
Pongo abelii	USNM 588109	F	L	USNM	—	—	NextEngine
Pongo abelii	UNSM 143588	M	L	USNM	—	—	NextEngine
Pongo abelii	USNM 143587	M	L	MS	M56592-101878	http://n2t.net/ark:/65665/33bd6f2f4-8b1a-4ffd-966f-06506fd24428	—
Pongo abelii	USNM 143590	M	L	MS	M56324-101610	http://n2t.net/ark:/65665/389dc210f-f5b3-4910-ae87-a26700227801	—
Pongo abelii	USNM 143593	M	L	MS	M56494-101780	http://n2t.net/ark:/65665/329ae2628-4c93-4da7-8e52-5f0c1e7bcc9e	—
Pongo abelii	USNM 143594	M	L	MS	M56426-101712	http://n2t.net/ark:/65665/3a893123e-021c-4f9b-ab42-4b4050332c24	—
Pongo abelii	USNM 143596	F	L	MS	M56423-101709	http://n2t.net/ark:/65665/3c26ea641-6662-42df-9b0d-a288ade0d69c	—
Pongo pygmaeus	AMNH 200900	F	L	AMNH	—	—	NextEngine
Pongo pygmaeus	USNM 142169	F	L	USNM	—	—	NextEngine
Pongo pygmaeus	USNM 145302	F	L	USNM	—	—	NextEngine
Pongo pygmaeus	USNM 153805	F	R	USNM	—	—	NextEngine
Pongo pygmaeus	USNM 153822	F	L	USNM	—	—	NextEngine
Pongo pygmaeus	ZMS 1982-0092	F	R	ZMS	—	—	µCT (BIR ACTIS)
Pongo pygmaeus	USNM 145301	M	L	USNM	—	—	NextEngine
Pongo pygmaeus	USNM 145305	M	L	USNM	—	—	NextEngine
Pongo pygmaeus	USNM 153823	M	L	USNM	—	—	NextEngine

Pongo pygmaeus	ZMS 1909-0801	M	L	ZMS	—	—	µCT (BIR ACTIS)
Pongo pygmaeus	ZMS 1966-0203	M	R	ZMS	—	—	µCT (BIR ACTIS)
Pongo pygmaeus	ZMB 87092	?	L	ZMB	—	—	µCT (BIR ACTIS)
Symphalangus syndactylus	AMNH 106583	F	L	AMNH	—	—	NextEngine
Symphalangus syndactylus	NMNH 271048	F	L	USNM	—	—	NextEngine
Symphalangus syndactylus	AMNH 106581	M	L	AMNH	—	—	NextEngine
Symphalangus syndactylus	PSU 105-1841	?	L	MS	M45351-82643	—	—
Symphalangus syndactylus	UWBM 58721-1	?	R	MS	M69298-125011	—	—
Symphalangus syndactylus	UWBM 82801-1	?	L	MS	M69299-125019	—	—
Symphalangus syndactylus	ZMB 38573	?	R	ZMB	—	—	µCT (BIR ACTIS)
Symphalangus syndactylus	ZMB 38587	F	L	ZMB	—	—	µCT (BIR ACTIS)

Abbreviations: F = female; M = male; ? = unknown sex; L = left; R = right; AMNH = American Museum of Natural History, New York, USA; CMNH = Cleveland Museum of Natural History, Cleveland, USA; MPI-EVA = Max Planck Institute for Evolutionary Anthropology, Leipzig, Germany; MS = MorphoSource.org; PCM = Powell-Cotton Museum, Birchington, UK; RMCA = Royal Museum for Central Africa, Tervuren, Belgium; SBU = Stony Brook University, New York, USA; USNM = Smithsonian National Museum of Natural History, Washington D.C., USA; ZMB = Museum für Naturkunde – Leibniz Institute for Evolution and Biodiversity Science, Berlin, Germany; ZMS = Zoologische Staatssammlung Munchen, Munich, Germany.

SOM Table S3

Landmark (L) and semilandmark (SL) protocol for KNM-BG 40021.[a]

L/SL no.	Description
Fovea capitis	
L1	Most medial point on fovea capitis outline
L2	Most anterior point on fovea capitis outline
L3	Most lateral point on fovea capitis outline
SL1	Midpoint between L1 and L2 on fovea outline
SL2	Midpoint between L2 and L3 on fovea outline
Radial head	
L4	Most medial point on radial head outline
L5	Most anterior point on radial head outline
L6	Most lateral point on radial head outline
SL3	Midpoint between L4 and L5 on radial head outline
SL4	Midpoint between L5 and L6 on radial head outline
L7	Most medial point on distal articular expansion of the radial head
L8	Most anterior point on distal articular expansion of the radial head
L9	Most lateral point on distal articular expansion of the radial head
SL5	Midpoint between L7 and L8 on distal articular expansion of the radial head
SL6	Midpoint between L8 and L9 on distal articular expansion of the radial head

[a] True landmarks (type II) and semilandmarks follow the descriptions of Bookstein (1997) and O'Higgins (2000).

SOM Table S4

Number of correctly classified specimens (and percentages within parentheses) by the bgPCA for extant taxa without cross-validation.

Taxon	Cercopithecines	Colobines	Hominids	Hylobatids	Platyrrhines
Cercopithecines	12 (75.0%)	0 (0%)	1 (6.3%)	0 (0%)	3 (18.8%)
Colobines	0 (0%)	6 (75.0%)	0 (0%)	0 (0%)	2 (25.0%)
Hominids	0 (0%)	0 (0%)	48 (81.4%)	9 (15.2%)	2 (3.4%)
Hylobatids	0 (0%)	0 (0%)	0 (0%)	14 (100%)	0 (0%)
Platyrrhines	1 (5.3%)	3 (15.8%)	2 (10.5%)	0 (0%)	13 (68.4%)

bgPCA = between-group principal component analysis.

SOM Table S5

Number of correctly classified specimens (and percentages within parentheses) by the bgPCA for extant taxa with cross-validation.

Taxon	Cercopithecines	Colobines	Hominids	Hylobatids	Platyrrhines
Cercopithecines	11 (68.7%)	1 (6.2%)	1 (6.25%)	0 (0%)	3 (18.7%)
Colobines	0 (0%)	6 (75,0%)	0 (0%)	0 (0%)	2 (25,0%)
Hominids	0 (0%)	0 (0%)	45 (76.3%)	11 (18.6%)	3 (5.1%)
Hylobatids	0 (0%)	0 (0%)	2 (14.3%)	12 (85.7%)	0 (0%)
Platyrrhines	2 (10.5%)	4 (21.0%)	3 (15.8%)	0 (0%)	10 (52.6%)

bgPCA = between-group principal component analysis.

SOM References

Adams, D.C., Collyer, M.L. 2016. On the comparison of the strength of morphological integration across morphometric datasets. Evolution 70, 2623–2631.

Adams, D.C., Collyer, M.L., Kaliontzopoulou, A., 2020. Geomorph: Software for geometric morphometric analyses. R package version 3.2.1. https://cran.r-project.org/package=geomorph.

Arias-Martorell, J., Almécija, S., Urciuoli, A., Nakatsukasa, M., Moyà-Solà, S., Alba, D.M., 2021. A proximal radius of *Barberapithecus huerzeleri* from Castell de Barberà: Implications for locomotor diversity among pliopithecoids. J. Hum. Evol. 157, 103032.

Blomberg, S.P., Garland, T., Ives, A.R., 2003. Testing for phylogenetic signal in comparative data: behavioral traits are more labile. Evolution 57, 717–745.

Bookstein, F.L., 1997. Landmark methods for forms without landmarks: Localizing group differences in outline shape. Med. Imaging Anal. 1, 225–243.

Freckleton, R.P., Harvey, P.H., Pagel, M., 2002. Phylogenetic analysis and comparative data: A test and review of evidence. Am. Nat. 160, 712–726.

Le Gros Clark, W.E., Thomas, D.P., 1951. Associated jaws and limb bones of *Limnopithecus macinnesi*. Fossil Mammals Afr. 3, 1–27.

O'Higgins, P., 2000. The study of morphological variation in the hominid fossil record: biology, landmarks and geometry. J. Anat. 197, 103–120.

Pagel, M., 1999. Inferring the historical patterns of biological evolution. Nature 401, 877–884.

Rose, M.D., Leakey, M.G., Leakey, R.E.F., Walker, A.C., 1992. Postcranial specimens of *Simiolus enjiessi* and other primitive catarrhines from the early Miocene of Lake Turkana, Kenya. J. Hum. Evol. 22, 171–237.

Rossie, J.B., Gutierrez, M., Goble, E., 2012. Fossil forelimbs of *Simiolus* from Moruorot, Kenya. Am. J. Phys. Anthropol. 147 (S54), 252.

Senut, B., 1989. Le Coude des Primates Hominoïdes. Anatomie, Fonction, Taxonomie, Évolution. Éditions du Centre National de la Recerche Scientifique, Paris.

Sherwood, R.J., Ward, R.J., Hill, A., Duren, D.L., Brown, B., Downs, W., 2002. Preliminary description of the *Equatorius africanus* partial skeleton KNM-TH 28860 from Kipsaramon, Tugen Hills, Baringo District, Kenya. J. Hum. Evol. 42, 63–73.

Walker, A.C., Pickford, M., 1983. New postcranial fossils of *Proconsul africanus* and *Proconsul nyanzae*. In: Ciochon, R.L., Corruccini, R.S. (Eds.), New Interpretations of Ape and Human Ancestry. Plenum Press, New York, pp. 325–351.

Ward, S., Brown, B., Hill, A., Kelley, J., Downs, W., 1999. *Equatorius*: A new hominoid genus from the middle Miocene of Kenya. Science 285, 1382–1386.

Zapfe, H., 1958. The skeleton of *Pliopithecus (Epipliopithecus) vindobonensis* Zapfe and Hürzeler. Am. J. Phys. Anthropol. 16, 441–457.

Zapfe, H., 1961. Die Primatenfunde aus der miozänen Spaltenfüllung von Neudorf an der March (Děvínská Nová Ves), Tschechoslowakei. Schweizer. Palaeontol. Abh. 78, 1–293.

Zelditch, M. L., Swiderski, D. L., Sheets, H. D., 2012. Geometric morphometrics for biologists: A primer. New York, Academic Press.